Critical Behavior and Extended States in 2D and 3D Systems with Gas-like Disorder

D. J. Priour, Jr^1

¹Department of Science, Kansas City Kansas Community College, Kansas City, Kansas 66112, USA (Dated: November 9, 2018)

With a tight binding treatment we examine amorphous conductors with gas-like disorder, or no correlations among the site positions. We consider an exponentially decaying hopping integral with range l, and the Inverse Participation Ratio (IPR) is used to characterize carrier wave functions with respect to localization. With the aid of two complementary finite size scaling techniques to extrapolate to the bulk limit (both methods exploit critical behavior in different ways to find the boundary between domains of extended and localized wave functions) which nevertheless yield identical results, we obtain phase diagrams showing regions where states are extended and domains of localized states. In the 2D case, states are localized below a threshold length scale l_c on the order of the interparticle separation $\rho^{-1/2}$ with a finite fraction of states extended for $l > l_c$. For D = 3, the extended phase is flanked by regions of localized states and bounded by two mobility edges. The swath of extended states, broad for $l \sim 1$, becomes narrower with decreasing l, though persisting with finite width even for $l < \frac{1}{5}\rho^{-1/3}$. Mobility edges are interpreted as lines of critical points, and we calculate the corresponding critical exponents.

PACS numbers: 72.15.Rn, 72.80.Ng, 71.23.-k, 71.23.An

The Anderson model [1], with disorder manifested as random perturbations in the site potential (i.e. diagonal disorder) has provided a way to examine localization effects in the context of a tight binding treatment. However, off-diagonal disorder where there are stochastic variations in the tunneling matrix elements also is germane to situations examined in experiment [2] and theoretical studies [3-7] which have also included calculations of the energy density of states (DOS) [8–10] and aspects of localization for 3D geometries [11–15]. Our aim is to determine conditions for the existence of extended states (system spanning wave functions amenable to charge transport) in the presence of very strong disorder where there is no correlation among site positions, a circumstance known as gas-like disorder [16] and also termed topological disorder due to the absence of a specific underlying lattice geometry.

Setting the constant diagonal terms to zero, we consider the tight binding Hamiltonian

$$\mathcal{H} = -\frac{1}{2}t_0 \sum_{i=1}^{N} \sum_{j \neq i} V(r_{ij}) (\hat{c}_i^{\dagger} \hat{c}_j + \hat{c}_i \hat{c}_j^{\dagger})$$
 (1)

where the sum over the index "i" ranges over the N particles contained in the simulation volume, we take the hopping parameter t_0 to be 3.0 electron volts, and the factor of "1/2" compensates for multiple counting. The operators \hat{c}^{\dagger} and \hat{c} create and destroy occupied electronic orbitals at sites indicated by the subscript. For the hopping integral, we use an exponential dependence $V(r_{ij}) = e^{-\gamma r_{ij}/s}$, where r_{ij} is the separation between sites i and j, $s = \rho^{-1/D}$ is the typical distance between neighboring sites, ρ is the volume density of sites, D is the dimensionality of the system, and γ is a dimensionless parameter. Since the length scale for the decay of the tunneling matrix element is $l = s/\gamma$, large/small γ val-

ues correspond to decay lengths small/large in relation to the typical interatomic separation. For the sake of convenience, we rescale coordinates such that $\rho=1$, with a simple inverse relationship $l=\gamma^{-1}$, and $V(r_{ij})=e^{-\gamma r_{ij}}$. Although the matrix element $V(r_{ij})$ is finite in range by virtue of the exponential decay, we nevertheless take into consideration hopping among all pairs of orbitals contained in the system of N sites with only a negligible increase in computational burden (i.e. a contribution on the order of N^2) relative to direct diagonalization used to calculate carrier states, which scales as N^3 .

With positional order (either locally or globally) not preserved in gas-like amorphous materials, the disorder strength is nonetheless characterized in a sense by the hopping integral decay scale l. For large l (small γ), the comparatively long-ranged tunneling connects sites to many neighbors, effectively averaging over hopping rates to and from many sites and mitigating the effect of strong disorder. However, if $l \ll 1$ (large γ), tunneling chiefly involves nearest neighbors. Hence, disorder is an a sense amplified for $\gamma \gg 1$ and muted if $\gamma \ll 1$, and one proceeds with the intuition that extended states are more likely to exist for larger l than for smaller l values.

For 2D systems, we find a threshold l_c where all states are localized for $l > l_c \sim 1$, with a finite portion of the wave functions extended for $l < l_c$. In the 3D case, a meta-study [2] of a large body of experiments in disparate systems corresponding to a broad range of γ values suggests a termination of conducting behavior for $\gamma > 3.8$. Nevertheless, though we find the portion of extended states to diminish monotonically in γ , we do not find an abrupt termination of the extended region for any particular value of γ , in contrast to D=2 where extended states do not exist if l is smaller than the interparticle separation. We construct phase diagrams show-

ing a region of extended states for intermediate energies bounded by two mobility edges; for a specific γ value, the latter are critical points marking a second order transition from the localized to extended phase at the lower edge and from extended to localized states at the upper edge.

To implement the numerical calculations, we examine a L^D supercell using periodic boundary conditions to mitigate finite size effects. A range of L values (i.e. as high as L=110 for D=2 and L=22 for D=3) are used to perform finite size scaling to determine if electronic states are localized or extended in the bulk limit. The Inverse Participation Ratio, $Y_2 = \sum_{i=1}^N |\psi_i|^4/(\sum_{i=1}^N |\psi_i|^2)^2$ shows distinct behavior depending on whether the wave functions tion is confined to a small volume (larger Y_2) or spread out over a larger region (smaller Y_2), and hence more extended in character. With a crystal lattice absent, one operates in the grand canonical ensemble, and the number of sites N varies about $\langle N \rangle = \rho L^D$ from sample to sample. In generating realizations of disorder, we account for fluctuations in the numbers of particles in an unbiased way using a technique described elsewhere [17]. To obtain adequate statistics, 10⁵ wave functions are retained for each combination of L and γ .

The random character of disorder precludes the study of the evolution of individual states with increasing L, and instead aggregates of wave functions must be examined. With carrier states parameterized by energy eigenvalues, one could in principle create partitions of width δE centered about uniformly spaced energies. However, since the energy density of states is sharply peaked [17], energy channels far from the central peak suffer from poor statistics. We ensure uniform statistics by using normalized rank $\tilde{r} = r/M$ (ranging from 0 to 1) to label carrier states, where M is the total number of states and r is the global eigenvalue rank within the large aggregate. For n = 100 partitions of the \tilde{r} domain, the channel width $\delta \tilde{r}$ is sufficiently small that systematic admixture effects from neighboring channels play a minor role, while still providing sufficient statistics for analysis, and parallel calculations for n = 50 and n = 200 yield results in quantitative agreement with the n = 100 scheme.

We calculate the channel averaged IPR in the thermodynamic limit as an avenue for the identification of mobility edges. For moderate to large L, we use a power law formula $Y_2(L) = Y_2^0 + A_1 L^{-\beta} + A_2 L^{-\delta}$ where Y_2^0 is the participation ratio in the bulk limit, β and δ are leading and next-to-leading order exponents, and A_1 and A_2 are amplitudes. The parameters Y_2^0 , β , δ , A_1 , and A_2 are fixed by a Monte Carlo nonlinear least squares fit to the channel averaged participation ratios.

Extrapolated participation ratios appear in Fig. 1 The troughs in the bulk Y_2 curves shown in panel (a) of Fig. 1 deepen with decreasing γ ; while IPR minima for $\gamma > 1.0$ are manifestly nonzero, participation ratios do seem to descend to zero for less rapid decay rates. Neverthe-

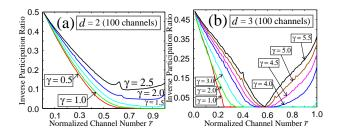


FIG. 1: (Color Online) Extrapolated Participation Ratio 2D and 3D results appear in panel (a) and panel (b), respectively for various γ values.

less, the gradual approach to the abscissa confounds a straightforward objective identification of a mobility edge for the 2D systems we examine.

Irrespective of γ , the D=3 extrapolated IPR curves in panel (b) Fig. 1 seem to plunge to zero and remain zero for a range of \tilde{r} values. However, the width of the interval where extended states seem to exist decreases with γ , with Y_2 appearing to vanish for most of the \tilde{r} domain in the case $\gamma = 1.0$ while only briefly touching the abscissa for $\gamma = 5.5$. For $\gamma < 3$ the IPR falls to zero with no subsequent return to finite values. On the other hand, for $\gamma \geq 3$, the interval of vanishing participation ratios is terminated for $\tilde{r} < 1$ as Y_2 abruptly rises to finite values. Salient feature not present in the 2D results are derivative discontinuities where Y_2 falls to zero, descending to or rising from the horizontal axis with a finite slope. The clear delineation of the regions where the IPR vanishes favors the use of basins in the Y_2 curves as a way to identify the boundary between extended and localized states in the 3D case.

With a complementary analysis, we calculate phase portraits showing localized and extended states for D=2and D=3. As a consequence of critical behavior at the mobility edge, one expects from single parameter finite size scaling theory a form $Y_2 = L^{\alpha_D} F_D[L^{1/\nu_D}(\tilde{r} - \tilde{r}_c)]$ near the boundary between regions of extended and localized states, with α_D and ν_D being critical exponents (ν_D controls the singular behavior of the correlation length ξ). Instead of trying to determine numerically where Y_2 falls to zero, the mobility edge is identified in an objective fashion by locating intersections of $\phi_2 \equiv Y_2(\tilde{r}, L)^{-1} L^{-\alpha_D}$, where α_D is fixed by insisting that curves for different system sizes L coincide, with \tilde{r}_c determined by the location of the crossing. A similar approach has been applied in theoretical studies of a 2D Anderson model with long-range correlated disorder [18] and Anderson localization of phonons [19] Data collapses, where ϕ_2 points plotted versus $L^{1/\nu_D}(\tilde{r}-\tilde{r}_c)$ for various L coincide on a single curve also are associated with a critical point, and in the case of the lower mobility edge are sharp enough to permit the determination the critical index ν_D by optimizing the data collapse.

Across the range of γ examined, we find from the ϕ_2

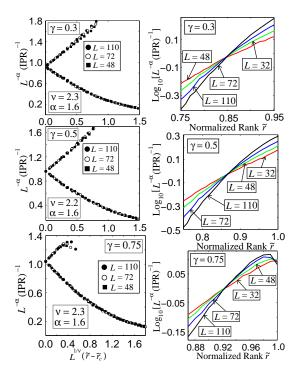


FIG. 2: (Color Online) Data collapse plots for (top to bottom) $\gamma = 0.3$, $\gamma = 0.5$, and $\gamma = 0.75$ appear on the left with the corresponding ϕ_2 intersections displayed on the right for D=2.

curve crossings that $\alpha_{2d} = 1.6 \pm 0.1$ for D = 2 and $\alpha_{\rm 3d} = 1.25 \pm 0.15$ for D = 3. In the 2D case, a mobility edge is identified only for $\gamma < 1$, and in the right panels of Fig. 2, ϕ_2 intersections for four distinct L values are shown for $\gamma = \{0.3, 0.5, 0.75\}$. The left panels show good data collapses for $\nu_{2d}(\gamma = 0.3) = 2.3 \pm 0.2$, $\nu_{\rm 2d}(\gamma = 0.5) = 2.2 \pm 0.2$, and $\nu_{\rm 2d}(\gamma = 0.75) = 2.3 \pm 0.2$ The ν_{2d} exponents in each case are identical within the bounds of error, in accord with the Harris Criterion. Although only one intersection appears for $\gamma = 0.3$ and $\gamma = 0.5$, the ϕ_2 curves appear to intersect twice for $\gamma = 0.75$ with the second crossing near $\tilde{r} = 1.0$. The incipient upper mobility edge is mirrored in the data collapse, which for $\gamma = 0.75$ is defocused in the vicinity of $\tilde{r} = 1.0$, where the scaling of Y_2 is controlled by the critical point marking the upper mobility edge.

A similar treatment identifies mobility boundaries for D=3, and the corresponding ϕ_2 data collapses and intersections are shown in Fig. 3. For $\gamma<2.5$, only a single intersection marks the boundary between localized states for $\tilde{r}<\tilde{r}_c$ and extended states for $\tilde{r}>\tilde{r}_c$. On the other hand, two sets of ϕ_2 intersections may be discerned for $\gamma>2.5$, indicating two distinct mobility edges with an interval of extended states flanked by localized states for $\tilde{r}<\tilde{r}_c^{\text{lower}}$ and $\tilde{r}>\tilde{r}_c^{\text{upper}}$. In the context of a similar tight binding model, a calculation by J. J. Krich and A. A-Guzik [14] has also identified two sets of mobility edges for D=3. The case $\gamma=2.5$ is marginal, since the

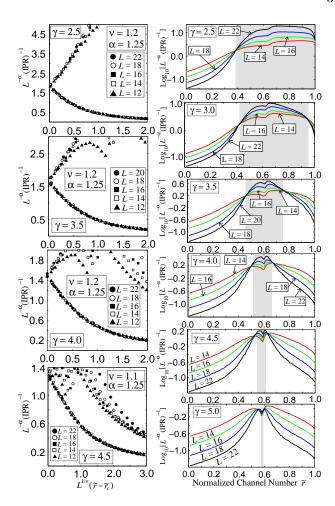


FIG. 3: (Color Online) Data collapse plots for various γ values (γ increases from top to bottom); data collapse plots corresponding to the lower mobility edge appear on the left, with ϕ_2 intersection plots shown on the right for D=3.

upper intersection appears to coincide with the upper \tilde{r} extreme, $\tilde{r} = 1$. The convergence of the mobility edges, and the concomitant constriction of the extended region affects the upper part of the data collapses calculated for the lower mobility edges where the severity of the defocusing increases with the proximity of the critical points in the upper mobility boundary. The areas in the right panels marked in gray match the \tilde{r} domains between intersections of ϕ_2 curves, and are determined from the extrapolated IPR results in Fig. 1, where we adopt the criterion $Y_2 \leq 10^{-3}$ for the presence of extended states. For the lower mobility edge, scaling collapses are sharp enough to be of service in fixing the exponent ν_{3d} , with results shown in Table I. As in the 2D case, within error bounds, the critical indices are in agreement across the broad range of γ values under consideration.

Phase diagrams showing regions of extended and localized states for D=2 appear in Fig. 4, where the main graph shows results in terms of the normalized rank \tilde{r} , and the inset is a phase portrait expressed in terms of the

γ	1.0	1.5	2.0	2.5	3.0
ν_{3d}	1.1 ± 0.15	1.2 ± 0.15	1.2 ± 0.15	1.2 ± 0.15	1.3 ± 0.15
γ	3.5	4.0	4.5	5.0	
ν_{3d}	1.2 ± 0.15	1.2 ± 0.15	1.1 ± 0.15	1.0 ± 0.2	

TABLE I: ν_{3d} results with for various γ values

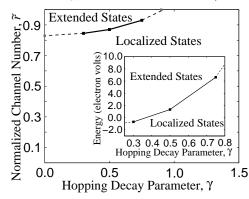


FIG. 4: Phase portraits for D=2 in terms of the normalized channel number \tilde{r} . The inset phase diagram is calculated with respect to energy. Filled symbols are calculated, and broken lines are extrapolations.

carrier state energies. Extended states occupy the upper left corner of the phase diagram, for $\gamma < 1.0$ and in the upper E and \tilde{r} ranges.

Phase portraits rendered in terms of \tilde{r} and E for the 3D case appear in the upper half of Fig. 5; mobility edges calculated from ϕ_2 intersections and gleaned from bulk Y_2 values appear in black and gray, respectively; the close overlap is a sign of excellent agreement among results of

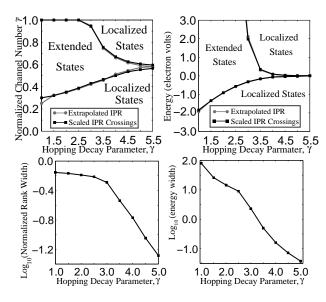


FIG. 5: Phase portraits for D=3 are shown in the upper row; mobility edges obtained from scaled IPR curve intersections and extrapolated participation ratios appear on the same graph. The logarithm of the width of the extended zone is graphed with respect to γ in the lower panels

the two very distinct methods of locating mobility edges, and serves to validate the use of bulk Y_2 results in constructing phase diagrams for 3D systems. The lower part of Fig. 5 contains graphs of the logarithm of the widths $w_{\tilde{r}}(\gamma)$ and $w_{\rm E}(\gamma)$ of the interval of extended states. Although the extended region grows rapidly narrower for $\gamma \geq 3.0$, there is no indication of an abrupt termination for finite l; the widths, within the bounds of error, both are consistent with an asymptotically exponential scaling $e^{-A/l}$ for $l \ll 1$.

In conclusion, we have obtained phase diagrams for 2D and 3D amorphous systems with gas-like disorder, finding extended states to be supported in the upper part of the energy range for D=2 above a threshold range $l_c\sim 0.9$ with the appearance of a second mobility edge near l_c . On the other hand, for D=3, we find a region of extended states even for $l\ll 1$ with no evidence for a termination of the extended phase for finite l. Mobility edges are interpreted as lines of critical points, which we have characterized by calculating the corresponding critical exponents.

Useful discussions with E. H. Hwang, J. Biddle, B. Wang, and S. Das Sarma are acknowledged. The numerical analysis has benefited from use of the University of Maryland, College Park HPCC computational facility.

- [1] P. W. Anderson, Phys. Rev. 109, 1492 (1958).
- [2] P. P. Edwards and M. J. Sienko, Phys. Rev. B 17, 2575 (1978).
- [3] F. J. Dyson, Phys. Rev. **92**, 1331 (1953).
- [4] R. Gade, Nucl. Phys. B **398**, 499 (1993).
- [5] D. A. Parshin and H. R. Schober, Phys. Rev. B 57, 10232 (1998).
- [6] V. Z. Cerovski, Phys. Rev. B 62, 12775 (2000).
- [7] K. Takahashi and S. Iida, Phys. Rev. B **63**, 214201 (2001).
- [8] D. E. Logan and M. D. Winn, J. Phys. C 21, 5773 (1988).
- [9] M. D. Winn and D. E. Logan, J. Phys.: Condens. Matter 1, 1753 (1989).
- [10] I. J. Bush, D. E. Logan, P. A. Madden, and M. D. Winn, J. Phys.: Condens. Matter 1, 2551 (1989).
- [11] W. Y. Ching and D. L. Huber, Phys. Rev. B 25, 1096 (1982).
- [12] A. Blumen, J. P. Lemaistre, and I. Mathlouthi, J. Chem. Phys. 81, 4610 (1984).
- [13] M. K. Gibbons, D. E. Logan, and P. A. Madden, Phys. Rev. B 38, 7292 (1988).
- [14] J. J. Krich, A. Aspuru-Guzik, Phys. Rev. Lett. 106, 156405 (2011).
- [15] S.-J. Xiong and S. N. Evangelou, Phys. Rev. B 64, 113107 (2001).
- [16] J. M. Ziman, Models of Disorder: The Theoretical Physics of Homogeneously Disordered Systems, Cambridge University Press, P. 472, (1979).
- [17] D. J. Priour, Jr., cond-mat 1004.4366 (2010).
- [18] I. F. dos Santos, F. A. B. F. de Moura, M. L. Lyra, and M. D. Coutinho-Filho, J. Phys.: condens. Matter 19,

(2010).

476213 (2007). [19] C. Monthus and T. Garel, Phys. Rev. B $\bf 81$, 224208